High-frequency climatic fluctuations over the past 30 ka in northwestern margin of the East Asian monsoon region, China

WU Huining[1*], CUI Qiaoyu[2*]

[1] Bailie School of Petroleum Engineering, Lanzhou City University, Lanzhou 730070, China;
[2] Key Laboratory of Land Surface Pattern and Simulation, Institute of Geographical Sciences and Natural Resources Research, Chinese Academy of Sciences, Beijing 100101, China

Abstract: Whether millennial- to centennial-scale climate variations throughout the Holocene convey universal climate change is still widely debated. In this study, we aimed to obtain a set of high-resolution multi-proxy data (1343 particle size samples, 893 total organic carbon samples, and 711 pollen samples) from an alluvial-lacustrine-aeolian sequence based on an improved age-depth model in the northwestern margin of the East Asian monsoon region to explore the dynamics of climate changes over the past 30 ka. Results revealed that the sequence not only documented the major climate events that corresponded well with those reported from the North Atlantic regions but also revealed many marked and high-frequency oscillations at the millennial- and centennial-scale. Specifically, the late stage of the last glacial lasting from 30.1 to 18.1 cal. ka BP was a dry and cold period. The deglacial (18.1–11.5 cal. ka BP) was a wetting (probably also warming) period, and three cold and dry excursions were found in the wetting trend, i.e., the Oldest Dryas (18.1–15.8 cal. ka BP), the Older Dryas (14.6–13.7 cal. ka BP), and the Younger Dryas (12.5–11.5 cal. ka BP). The Holocene can be divided into three portions: the warmest and wettest early portion from 11.5 to 6.7 cal. ka BP, the dramatically cold and dry middle portion from 6.7 to 3.0 cal. ka BP, and the coldest and driest late portion since 3.0 cal. ka BP. Wavelet analysis results on the total pollen concentration revealed five substantially periodicities: c. 5500, 2200, 900, 380, and 210 a. With the exception of the c. 5500 a quasi-cycle that was causally associated with the Atlantic meridional overturning circulation, the other four quasi-cycles (i.e., c. 2200, 900, 380, and 210 a) were found to be indirectly causally associated with solar activities. This study provides considerable insight into the dynamic mechanism of the Asian climate on a long-time scale and future climatic change.

Keywords: East Asian monsoon region; total pollen concentrations; climate periodicity; millennial-centennial time scale; Chinese Loess Plateau

Citation: WU Huining, CUI Qiaoyu. 2022. High-frequency climatic fluctuations over the past 30 ka in northwestern margin of the East Asian monsoon region, China. Journal of Arid Land, 14(12): 1331–1343. https://doi.org/10.1007/s40333-022-0037-5

1 Introduction

The study of past climate change has improved prior understanding of the mechanisms of the Earth's climate system (Ren et al., 2021). Climate change is unstable and quasi-periodic over longer timescales. Exploring the periods and mechanisms of climate change over longer timescales can not only contribute to the understanding of patterns and causes of past climate change, but more importantly provide a scientific reference for predicting future climate and

*Corresponding authors: WU Huining (E-mail: wuhn510@163.com); CUI Qiaoyu (E-mail: qiaoyu.cui@igsnrr.ac.cn)
Received 2022-06-09; revised 2022-10-31; accepted 2022-11-14

environmental changes. In recent years, different millennial-, centennial-, and decadal-scale quasi-periods have been found in high-resolution paleoclimate proxies from ice cores, stalagmites, tree rings, loess-paleosol, and lacustrine sediments. These quasi-periodic signals in climate change over different time scales may be linked to periodic signals of solar activity (Kravchinsky et al., 2013; Soon et al., 2014; Zhao and Feng, 2014; Zhang et al., 2017; Huang and Tian, 2018). However, these studies primarily focused on the Holocene or middle and late Holocene. Accordingly, only few studies have been conducted on the periodicity of longer time sequences of high-resolution climate proxies prior to the Holocene. Therefore, whether the millennial- to centennial-scale climate variations of the last 1×10^4 a convey universal climate change or merely represent a characteristic of the Holocene remain unknown (Kravchinsky et al., 2021).

The Earth's climate systems have experienced multiple major changes over the past 30 ka, primarily including the Last Glacial Maximum (LGM), the Last Deglaciation, and the Holocene Climatic Optimum. Superimposed on these major changes were abrupt oscillations at millennial- and centennial-scale (e.g., Heinrich Events, D-O (Dansgaard-Oeschger) Oscillations, and Holocene Bond Events). To explore the mechanisms related to these major changes and abrupt oscillations, we needed high-quality data (i.e., high-resolution sampling, well-dated chronology, and adequately defined proxy) from locations that represent different geographic settings. Many high-quality palaeoclimate sequences covering the past 30 ka have already been retrieved from various geographic settings, and these sequences have already revealed certain basic characteristics of large-scale climate change over the past 30 ka (Grootes et al., 1993; Bond et al., 1997, 1999; Liu et al., 2001; Wang et al., 2001; Dykoski et al., 2005; An et al., 2012). However, the locations of the reported sequences were not evenly distributed geographically. In particular, studies are lacking in mid-latitude regions that link high-latitude climate systems with low-latitude climate systems. To further improve our understanding of those major changes and abrupt oscillations, researchers must retrieve more high-quality palaeoclimate sequences (especially high resolution palaeovegetation records) from the mid-latitude regions, especially from the margin of the East Asian monsoon region that is extremely sensitive to large-scale climate changes (Yang et al., 2019). Accordingly, the western part of the Chinese Loess Plateau, situated in the margin of the East Asian monsoon region, deserves more attention.

In this study, we aimed to re-examine previously reported major climatic and environmental changes (Wu et al., 2009; Sun and Feng, 2015; Wu et al., 2020) with an improved chronology, and explore the periodicities of the abrupt climatic and environmental oscillations expressed by the data (e.g., particle size, total organic matter content, and pollen record) retrieved from an alluvial-lacustrine-aeolian sequence in the western part of the Chinese Loess Plateau.

2 Materials and methods

2.1 Physiographic settings

This study sought to focus on the Xiaogou (XG) section (36°01′12″N, 104°59′24″E; 1625 m a.s.l.; Fig. 1), an alluvial-lacustrine-aeolian sequence in the western part of the Chinese Loess Plateau. This area is located in the conjunctional zone of three major geographical regions of China: the humid monsoon region in the east, the arid region in the northwest, and the alpine-cold region on the Qinghai-Tibet Plateau. The western part of the Chinese Loess Plateau is topographically characterized by ridges and valleys, with elevations ranging from 1200 to 2500 m a.s.l. and climatically characterized by continental and semi-arid/semi-humid types. The annual mean temperature ranges from 6℃ to 10℃ in the Huajialing Mountains. However, the mean annual precipitation markedly differs between the southeast (500–550 mm) and northwest (200–500 mm) in the Huajialing Mountains. Accordingly, the zonal vegetation in the southeast is temperate semi-humid forest or sparse forest steppe, whereas that in the northwest is temperate semi-arid and arid steppe (Wu et al., 1980). The dominant tree species in this region are *Quercus liaotungensis* Koidz., *Populus davidiana* Dode, *Betula platyphylla* Suk., *Platycladus orientalis* (Linn.) Franco, *Pinus tabuliformis* Carr., and *Picea asperata* Mast., which primarily remain in the valleys (Chen et al., 2000).

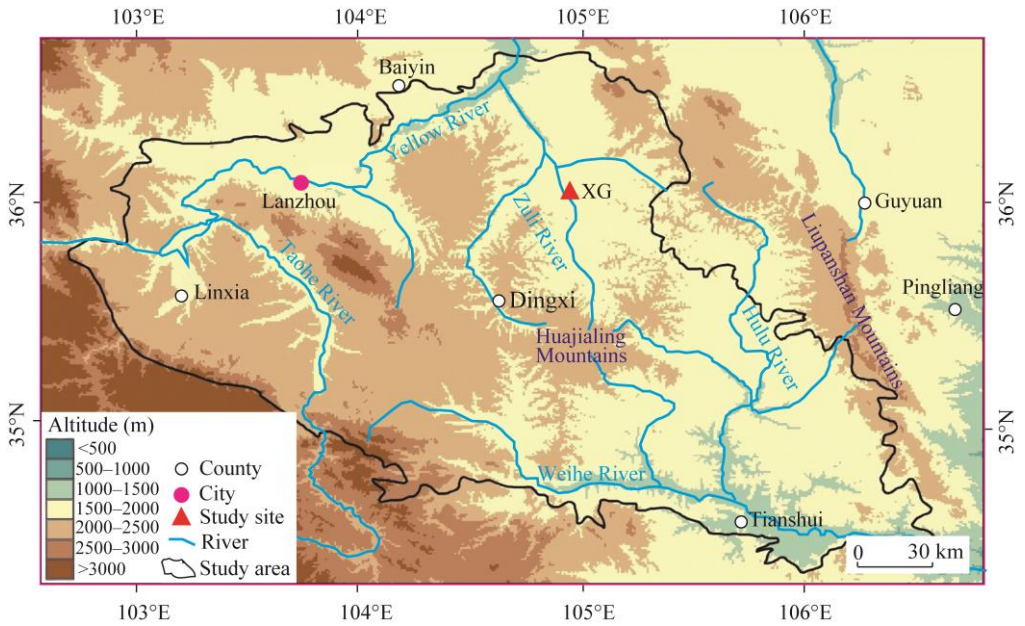

Fig. 1 Geographic location of the study area and XG (Xiaogou) section

2.2 Sedimentary facies and improved age-depth model

The studied section (XG section) is a 40-m thick outcropping sediments along the Zuli River that is a major tributary of the Yellow River. According to the lithofacies characteristics (e.g., color, lithology, and structure of sedimentation), we divided the section into the following five stratigraphic units from bottom to top (Fig. 2): (1) floodplain facies (40.0–32.4 m: brown-yellowish silt and clayey silt layer underlain by a gravel layer at the bottom), (2) shallow lake facies (32.4–21.8 m: light-black silty-clay and brown-yellowish silt alternating stratification), (3) deep lake facies (21.8–7.3 m: dark-black, light-black clay/silty-clay and brown-yellowish silt alternating stratification), (4) shallow lake facies (7.3–2.6 m: light-black, grey-greenish silty-clay, and brown-yellowish silt alternating stratification), and (5) aeolian loess (2.6–0.0 m: a massive and yellowish clayey silt layer) (Wu et al., 2020). In the field, the lake-facies portion (32.4–2.6 m, units 2–4) was formed at the outlet of the basin under a completely closed terminal lake when the Zuli River was dammed by a massive landslide (Wu et al., 2009, 2020).

A total of 23 ^{14}C dates (Table 1), including 19 previously reported dates (Wu et al., 2009), and four newly obtained dates (i.e., AA87138, AA87139, AA87140, and AA87141 with * in Table 1), are now available, and all radiocarbon dates were calibrated to calendar years using IntCal20 (Reimer, 2020). After adding new dating data, we improved the original age-depth relationship model (Wu et al., 2009). The new age (A)-depth (D) model was established by adopting a unified nonlinear polynomial model for the calibrated dates, which is expressed as $A=1.2191\times10^{-3}D^3-6.2875\times10^{-2}D^2+1.3165D$ (R^2=0.9016) (Fig. 2). Based on this model, we extrapolated the age of the section bottom at a depth of 40 m to be approximately 30 cal. ka BP (calendar age before presentation). Despite the existence of several inversions among the ^{14}C ages, the newly established chronology of the XG section is reliable when the continuous deposition inferred from the horizontal layer structure of the XG section is considered (Fig. 2).

2.3 Materials and methods

The re-examined data employed in this study included 1346 grains-size data (with an average interval of 3 cm and an average resolution of 22 a/sample), 893 total organic carbon (TOC) data (with an average interval of 5 cm and an average theoretical resolution of 34 a/sample), and 711

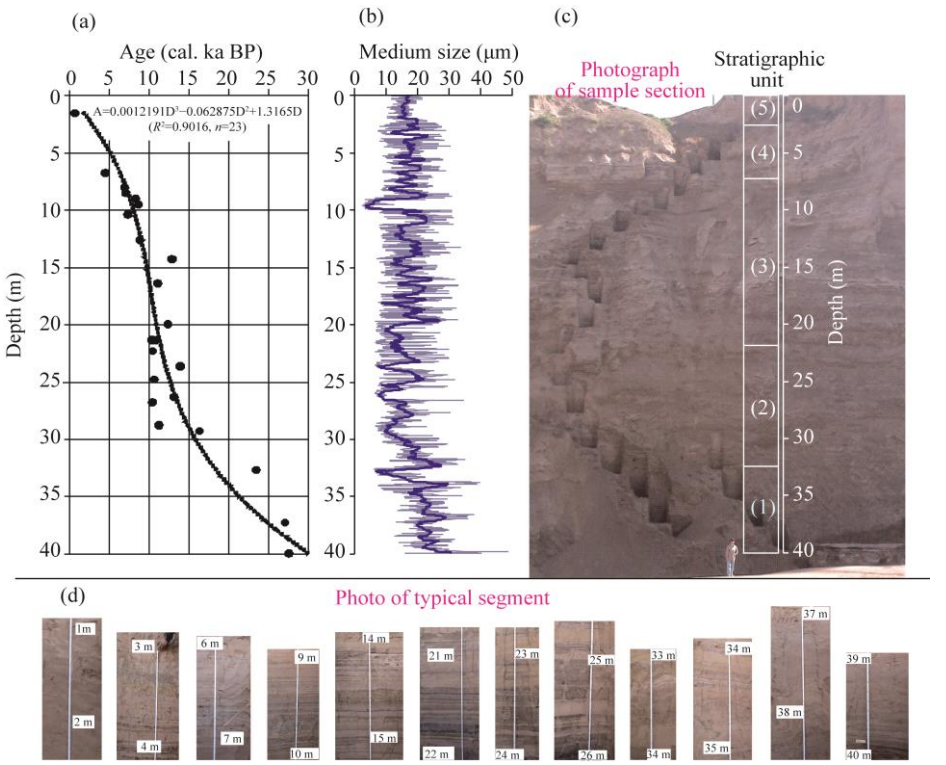

Fig. 2 (a), relationship between age and depth; (b), distribution curve of medium size (thick line represents the 5-point moving average trend line); (c and d), images of the alluvial-lacustrine-aeolian sequence of the XG (Xiaogou) section.

Table 1 ^{14}C dating data and correction age of the XG (Xiaogou) section

Laboratory number	Depth (cm)	^{14}C age (a BP)	Calibrated age (2σ) (cal. a BP)
[a]AA64267	152–154	803±40	671–752
[a]AA64268	674–675	4033±44	4413–4623
[a]AA87138*	800	6088±45	6840–7032
[a]AA87139*	850	6186±44	6954–7168
[a]AA87140*	900	7484±39	8194–8375
[a]AA87141*	950	7855±76	8517–8814
[a]AA64270	1036–1037	6412±56	7254–7427
[a]AA64272	1258–1259	8039±72	8644–9035
[a]AA64275	2132–2133	9171±50	10,236–10,436
[a]AA64276	2226–2228	9292±79	10,252–10,662
[a]AA64277	2475–2478	9393±49	10,499–10,747
[a]AA64278	2674–2676	9210±110	10,195–10,608
[a]AA64279	2874–2876	9807±52	11,156–11,324
[b]LUG06-45	1426–1428	10,870±98	12,712–13,007
[b]LUG06-46	1636–1639	9782±118	10,761–11,413
[b]LUG06-47	1992–1996	10,487±123	11,993–12,716
[b]LUG06-48	2132–2136	9572±129	10,573–11,217
[b]LUG06-49	2360–2364	11,981±157	13,498–14258
[b]LUG06-50	2628–2632	11,259±107	12,921–13,346
[b]LUG06-51	2924–2928	13,501±162	15,805–16,807
[b]LUG06-100	3260–3272	19,421±191	23,016–23,786
[b]LUG06-101	3720–3732	22,811±246	26,457–27,580
[b]LUG06-102	3990–4000	23,243±272	27,103–27,886

Note: [a], AA samples (charcoal) dated at the NSF-Accelerator Mass Spectrometry (AMS) Laboratory Facility, University of Arizona, USA; [b], LUG samples (bulk) dated at the Key Laboratory of Western China's Environmental Systems, Ministry of Education, Lanzhou University, China. *, ^{14}C age data obtained after 2009.

pollen data (with an average interval of 6 cm and mean resolution of 42 a/sample), which have been described in previous studies (Wu et al., 2009, 2020).

Generally, a coarser particle-sized lacustrine sedimentary unit was formed during a drier period when the core site was closer to the lake water inlet because of lake shrinkage, and/or the drainage basin supplying water to the lake was poorly covered with vegetation (Chen et al., 2004; Shen et al., 2010). For loess, the medium size (Md) is an indicator of the winter monsoon intensity, and a coarser particle-sized loess unit is widely interpreted to indicate a drier or/and colder period when the winter monsoon is more intense (Ding et al., 1996; Chen et al., 1999). And, loess and lacustrine alternating sedimentary unit was interpreted to reflect periodical alternations between drier conditions (loess) and wetter conditions (lacustrine deposits) (Xia, 1992).

TOC content of lacustrine deposits normally reflects the input and retention of endogenous and exogenous organic matter, representing biological productivity within the lake and/or within the drainage basin supplying water to the lake. A higher TOC may indicate a better-vegetated drainage basin and/or a more productive lake environment (Shen et al., 2010). Consequently, TOC in those lacustrine sequences within the monsoon climate zones was interpreted to indicate vegetation coverage and biomass, thereby reflecting the amount of monsoon precipitation (Zhou et a1., 1996, 1999; Guo et al., 2002).

Warmer and wetter environments were characterized by a general increase in watershed vegetation coverage, which led to an increase in total pollen concentration (TPC). Thus, an increase in pollen concentration corresponds to a relatively warmer and wetter climate (Tarasov et al., 2009; Bezrukova et al., 2011; Kravchinsky et al., 2021). Variations in pollen concentration may reflect changes in vegetation coverage if both the plant composition and deposition rate are somewhat constant. Higher vegetation coverage in monsoonal areas was interpreted to indicate a higher effective humidity in the river basin (Li et al., 2000, 2003; Zhu, 2002; Shen et al, 2005; Chen et al, 2006; Luo et al., 2006).

Figure 3 shows that the pollen concentrations (including total, coniferous, deciduous, shrubs and herbs, and some representative generas) relatively align well with TOC and Md. Thus, higher values of TPC align with higher TOC values and lower Md values. Of note, all lacustrine sub-units within the lacustrine-dominated sedimentary facies units (i.e., units 2, 3, 4 in Fig. 2) are basically characterised by lower values in the Md and higher values not only in TOC, but also in TPC. Contrarily, all loess sub-units within the lacustrine-dominated sedimentary facies units (i.e., units 2, 3 and 4 in Fig. 2) are basically characterised by higher values in Md and lower values not only in TOC, but also in TPC (see the shaded strips in Fig. 3).

In summary, higher TPC and TOC, and lower Md indicate stronger summer monsoons, higher vegetation coverage, and warm-wetter climate. In contrast, lower TPC and TOC, and higher Md indicate a stronger winter monsoon, lower vegetation coverage, and relatively dry-colder climate.

3 Results and discussion

The history of regional vegetation and climate changes recorded by pollen and other climatic data in the XG section was previously discussed (Wu et al., 2009, 2020). Based on the improved age-depth model established in this study, the vegetation and climate history over the past 30 ka in the study region are briefly summarized in Table 2 (pollen zone, see Fig. 3). In general, vegetation in the study area is very sensitive to climate change, and the forest/sparse forest steppe zone has advanced and retreated many times from southeast to northwest since the LGM (Wu et al., 2020). When the summer monsoon is enhanced, the climate becomes wet and warm, leading to the advance of the forest/sparse forest steppe zone from southeast to northwest; when winter monsoon is enhanced, the climate becomes cold and dry, leading to the retreat of the forest/sparse forest steppe zone from northwest to southeast.

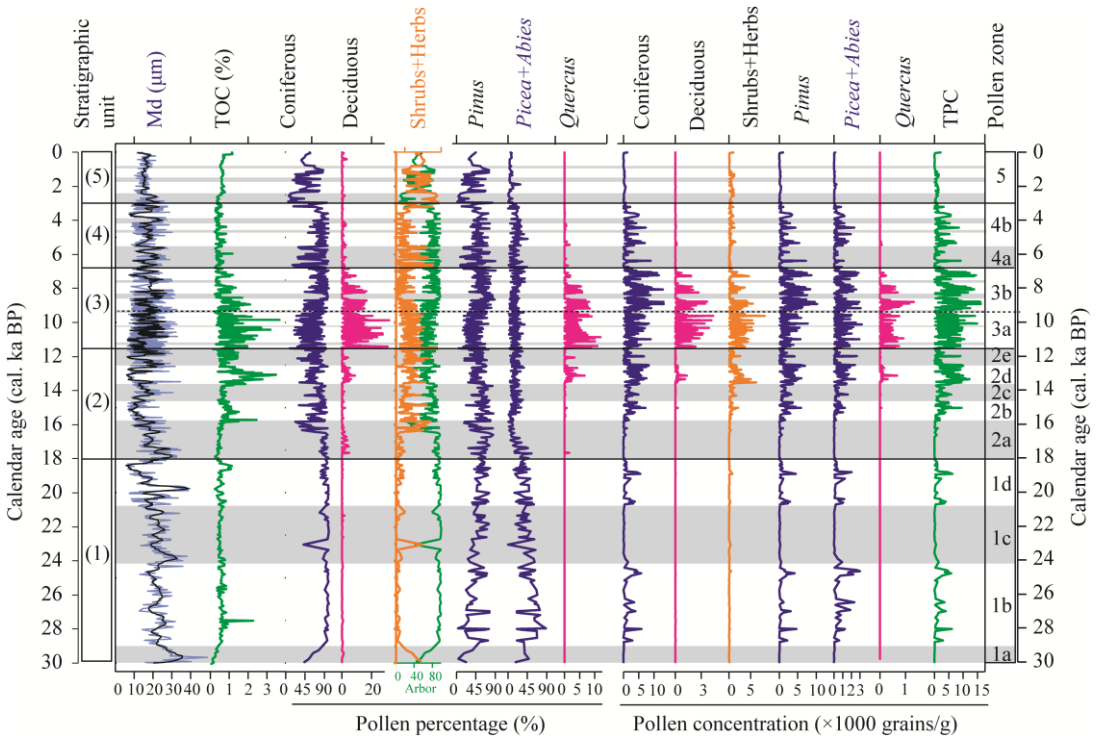

Fig. 3 Pollen percentage, pollen concentration (including coniferous trees, deciduous broad-leaved trees, shrubs and herbs, and representative genera (*Pinus*, *Picea+Abies*, and *Quercus*)), TPC (total pollen concentration), TOC (total organic carbon), and Md (medium size) (thick line represents the 5-point moving average trend line) of the XG (Xiaogou) section. Grey shaded band indicates relatively cold-dry time period.

Table 2 History of vegetation and climate change recorded by pollen in the XG (Xiaogou) section

Stratigraphic unit and depth (m)	Pollen zone and age	Vegetation	Climate
40.00–32.40	1a: 30.1–29.0 cal. ka BP	Desert steppe	Cold and dry
	1b: 29.0–24.2 cal. ka BP	Coniferous forests (*Picea*, *Abies*, and *Pinus*)	Relatively wet
	1c: 24.2–20.7 cal. ka BP	Desert steppe	Cold and dry
	1d: 20.7–18.1 cal. ka BP	Coniferous forests (*Picea*, *Abies*, and *Pinus*)	Relatively wet
32.40–21.80	2a: 18.1–15.8 cal. ka BP	Desert steppe	Dry and cold
	2b: 15.8–14.6 cal. ka BP	Coniferous sparse forest steppe	Relatively humid
	2c: 14.6–13.7 cal. ka BP	Steppe	Relatively cold and dry
	2d: 13.7–12.5 cal. ka BP	Coniferous forest steppe	Relatively warm and humid
	2e: 12.5–11.5 cal. ka BP	Steppe	Relatively cold and dry
21.80–7.25	3a: 11.5–9.4 cal. ka BP	Coniferous broad-leaved mixed forest	Warm and relatively wet
	3b: 9.4–6.7 cal. ka BP	Broad-leaved coniferous mixed forest	Wet and relatively warm
7.25–2.56	4a: 6.7–5.5 cal. ka BP	Steppe	Relatively cold and dry
	4b: 5.5–3.0 cal. ka BP	Coniferous sparse forest steppe	Relatively humid
2.56–0.00	5: 3.0–0.0 cal. ka BP	Steppe/desert steppe	Relatively dry and cold

Based on this finding, we opted to focus on the abrupt climatic change events recorded by TPC, TOC, and Md of the XG section over the past 30 ka, their occurrence cycles, and their possible mechanisms (Figs. 4 and 5).

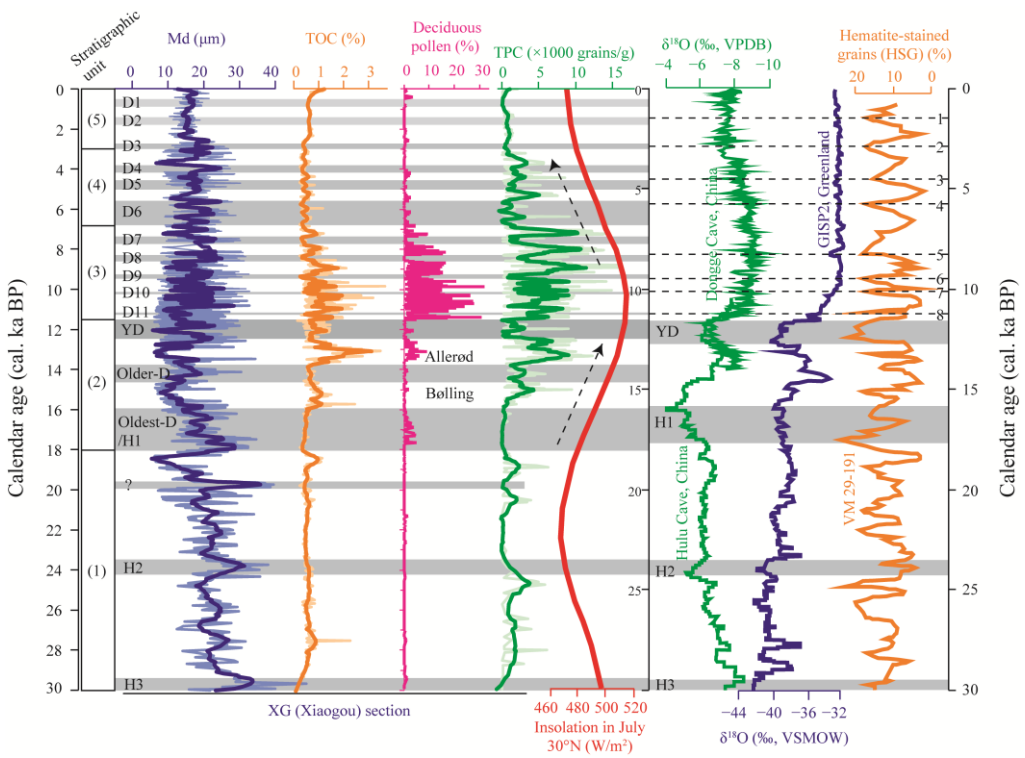

Fig. 4 Comparison of Md (medium size) (thick line represents the 5-point moving average trend line), TOC (total organic carbon), deciduous pollen percentage, and TPC (total pollen concentration) of the XG (Xiaogou) section with the haematite-stained grain content record from the North Atlantic deep-sea core (VM29–191, Bond et al., 1997), the oxygen isotopic record from the Greenland ice core (Grootes et al., 1993), the Hulu Cave stalagmite (Wang et al., 2001), the Dongge Cave stalagmite (Dykoski et al., 2005), and the summer insolation of the Northern Hemisphere (Berger, 1978). D1–D11 represent 11 Holocene dry events; 1–8 represent eight Holocene cold events; H1–H3 represent Heinrich-like events. YD, Younger Dryas; VSMOW, Vienna Standard Mean Ocean Water; VPDB, Vienna Pee Dee Belemnite.

3.1 Late Glacial and Heinrich Events

The floodplain facies (i.e., stratigraphic unit 1 in Figs. 2 and 3) was formed during the late stage of the last glacial, lasting from 30.1 to 18.1 cal. ka BP. The corresponding particle size reached the coarsest part of the entire section, with low TPC and TOC (Fig. 3). Such results indicate that the drainage basin of the Zuli River was rather poorly vegetated, and the associated loess hill-slope erosion effectively contributed to the floodplain deposits under extremely dry conditions, aligning with the results from other parts of the Chinese Loess Plateau (Ding et al., 1996). However, of note, this period (i.e., from 30.1 to 18.1 cal. ka BP) was not monotonously dry. Instead, two relatively humid intervals, which are characterized by relatively high values of coniferous pollen concentration and TOC, segmented this dry period into four epochs: a dry epoch in 30.1–29.0 cal. ka BP, a relatively wet epoch in 29.0–24.2 cal. ka BP, a dry epoch in 24.2–20.7 cal. ka BP, and a relatively wet epoch at 20.7–18.1 cal. ka BP (Fig. 3).

The curves of the proxy records from the XG section (i.e., Md, TOC, deciduous pollen percentage, and TPC) were compared with the $\delta^{18}O$ curves of the Hulu Cave stalagmite (Wang et al., 2001), the $\delta^{18}O$ curve from the Greenland ice core (Grootes et al., 1993), and the haematite-stained grain content curve from the North Atlantic deep-sea core (Bond et al., 1997) (Fig. 4). Figure 4 shows the three Heinrich or Heinrich-like events at 29.5, 23.8, and 19.7 cal. ka BP (the corresponding Md reaches the coarsest points with the low TPC and TOC). The first peak at 29.5 cal. ka BP appeared to correspond with the Heinrich Event 3 (i.e., H3), recorded not only from the North Atlantic region (i.e., deep-sea core and ice core) but also the Chinese stalagmite region (i.e., Hulu Cave), whereas the second peak at 23.8 cal. ka BP corresponded approximately to H2. The third peak at 19.7 cal. ka BP, which is short but unequivocally expressed in the XG

section, has no corresponding records from deep-sea and ice cores in the North Atlantic region.

3.2 Deglacial wetting and Dryas dry events

The shallow lake facies (i.e., stratigraphic unit 2 in Figs. 2 and 3) was formed during the last deglacial from 18.1 to 11.5 cal. ka BP. The declining trend of Md and the increasing trends of TOC and TPC indicate that the climate was wetting (the appearance of deciduous broad-leaved tree pollen by *Quercus* indicates potential warming, see Figs. 3 and 4) during the deglacial. The proxy records also documented several dry excursions (indicated by low values of TOC and TPC, but high values of Md) superimposed on the wetting trend. The first dry excursion lasted from 18.1 to 15.8 cal. ka BP, which corresponds well with the Heinrich Event 1 (i.e., H1 or the Oldest Dryas) (16.7 cal. ka BP) not only recorded in the North Atlantic region (i.e., deep-sea core and ice core) (Bond et al., 1997), but also in the Chinese stalagmites (i.e., Hulu Cave) (Wang et al., 2001). The proxy-documented dry interval was 14.6–13.7 cal. ka BP in the XG section corresponding to the Older Dryas cold event (14.2–13.7 cal. ka BP) retrieved from the Greenland ice core (Grootes et al., 1993). The proxy-documented dry interval of 12.5–11.5 cal. ka BP corresponds to the Younger Dryas event (12.7–11.5 cal. ka BP) retrieved from the Greenland ice core (Grootes et al., 1993) and the Chinese stalagmites (i.e., Hulu Cave and Dongge Cave) (Wang et al., 2001; Dykoski et al., 2005). Two intervening warm intervals retrieved from the North Atlantic region (Bond et al., 1997), namely the Bølling warm period and Allerød warm period (Stuiver et al., 1995; Li et al., 2004; Shen et al., 2005), were also documented in the proxy records (indicated by the higher values of TOC and TPC, but lower value of Md) in the XG section (Fig. 4).

3.3 Holocene Climatic Optimum and dry events

The deep lake facies (i.e., stratigraphic unit 3 in Figs. 2 and 3) formed during the period from 11.5 to 6.7 cal. ka BP. The highest average values of TOC and TPC and a relatively high average value of deciduous pollen percentage (Figs. 3 and 4) imply that this time might be the Holocene Climatic Optimum, with the warmest and wettest periods belonging to 9.5–6.7 cal. ka BP (the maximum TPC occurred at approximately 9.0 cal. ka BP). The shallow lake facies (i.e., stratigraphic unit 4 in Figs. 2 and 3) formed during the period lasting from 6.7 to 3.0 cal. ka BP overlies the deep lake facies. TOC and TPC values markedly decreased compared with those in the underlying deep lake facies (i.e., stratigraphic unit 3). This dry period (from 6.7 to 3.0 cal. ka BP) was most likely a cold period, as indicated by the nearly complete disappearance of deciduous pollen (Figs. 3 and 4). The aeolian loess deposition (i.e., stratigraphic unit 5 in Figs. 2 and 3) has dominated the XG section over the past 3000 a. Low values of TOC and TPC and an absolute lack of deciduous pollen suggest that the climate was dry and cold during the most recent 3000 a.

Eleven dry episodes (i.e., D1–D11 in Fig. 4) were superimposed on the aforementioned general patterns of the Holocene (i.e., the warmest and wettest early portion, dramatically cooled and dried middle portion, and the coldest and driest late portion). These dry episodes were pronouncedly and unequivocally expressed by the elevated values of Md and the lowered values of TOC and TPC. Notably, although these 11 Holocene dry episodes in the XG proxy records do not correspond well with the eight Holocene Bond events in the North Atlantic haematite-stained grain content record (Bond et al., 1997), these 11 dry episodes correspond to approximately 11 cold-dry events reported from nearby Sujiawan and Dadiwan sections in the western part of the Chinese Loess Plateau (Tang et al., 2007). Furthermore, the ice raft events recorded by floating ice debris in the North Atlantic are accompanied by relatively strong winter wind events in China; however, not all strong winter wind events have corresponding ice raft events (Chen et al., 2001). This finding also highlights the sensitivity and complexity of climate environment changes in the arid and semi-arid areas of China. Of note, 6.7–5.5 cal. ka BP (i.e., D6 in Fig. 4), a period of prolonged climatic deterioration in the middle Holocene, is similar to the Younger Dryas event.

4 Climate change cycles

The advantage of wavelet analysis for the detection of climatic periodicity has been demonstrated on numerous climatic records used to evaluate millennial and centennial cycles (Debret et al., 2009; Kravchinsky et al., 2021). TPC was a superposition of various pollen taxa in the record, and was sensitive to both temperature and moisture variations. TPC acted as a stacked climatic parameter that smoothed the record, but also balanced out some uncertainties related to individual reaction of particular taxa to specific short-term conditions (Kravchinsky et al., 2021). As shown in Figure 4, although the curves of TOC and TPC in the XG section are generally parallel to the curve of the summer insolation in the Northern Hemisphere (Berger, 1978), dramatic and frequent oscillations in the proxy records (i.e., Md, TOC, and TPC) can be readily observed throughout the entire XG section covering the past 30 ka. To explore the periodic characteristics of these dramatic and frequent oscillations, we used MATLAB to perform wavelet analysis (Torrence and Compo, 1998) on the TPC (2991 equal time spacing (10 a) time series data after interpolation) of the XG section. Wavelet analysis revealed five significant or high-confidence millennial- and centennial-scale periodicities: c. 5500, 2200, 900, 380, and 210 a (Fig. 5a). At 95% confidence, we extracted the filtering curves of c. 5500, 2200, 900, 380, and 210 a (Fig. 5b).

First, c. 5500 a quasi-cycle expressed in TPC data of the XG section is quite consistent with that of the Heinrich Events, which are causally associated with the Atlantic meridional overturning circulation (Grimm et al., 1993; Arbic et al., 2004), and roughly correspond to the classical Bond cycle (Zeng et al., 2019). Second, c. 2200 a quasi-cycle is quite similar to c. 2000 a cycles of ENSO (El Niño-Southern Oscillation) activity that might be associated with solar activity (Li et al., 2004; Wang, 2009), and correspond to the Dansgaard-Oeschger oscillation (Bond et al., 1999; Zeng et al., 2019), and very close to the reported quasi-cycle of c. 2162 a of the East Asian summer monsoon (Zhang et al., 2017), which also aligns with the Hallstatt cycle (2215–2400 a) of total solar radiation variation (Zhang et al., 2017; Huang and Tian, 2018). Third, c. 900 a quasi-cycle is consistent with the cycle of 1000 a (Eddy cycle) of sunspot number and total solar radiation variation (Clemens, 2005; Zhang et al., 2017; Huang and Tian, 2018), which is not only confirmed by large Holocene climatic records, but is also reflected by high-pollen resolution records from the Lake Kotokel in southern Siberia, Russia, during the LGM (Kravchinsky et al., 2021). Fourth, c. 380 a quasi-cycle is very close to c. 400 a quasi-cycle observed from the East Asian summer monsoon (Zhang et al., 2017), which may be equivalent to the unnamed period of approximately 350 a solar total radiation amount (Huang and Tian, 2018). Fifth, c. 210 a quasi-cycle might be a sensitive response to the Suess solar cycle (180–210 a, i.e., de Vries cycle) (Ojala et al., 2015), which is also reflected by the high-pollen resolution records in the LGM (Kravchinsky et al., 2021).

The following three points must be highlighted. First, the last three Heinrich events (H3, H2, and H1) occurred at the quasi-periodic trough of c. 5500 a, and the three Dryas events (Oldest Dryas, the Older Dryas, and the Younger Dryas) were basically consistent with a trough of c. 2200 a quasi-cycle. Second, three shorter quasi-cycles (i.e., c. 900, 380, and 210 a) can explain most of the dramatic oscillations in the total pollen concentration data. Third, chronological additions of these five quasi-cycles mimicked the TPC curve well (Fig. 5c). In addition, the wavelet transformation and filtering curve revealed that two millennial-scale quasi-periods (c. 5500 and 2200 a) were both stable and continuous for approximately 30 ka, indicating that these two periods are characteristic of regional climate change over the last 30 ka. The signal of a nearly millennial-scale quasi-cycle (c. 900 a) was weak in the LGM, gradually became stronger from the deglacial, and was continuously stable throughout the Holocene, which may be the main periodic signal for the Holocene. The signals of two shorter centennial-scale quasi-cycles (c. 380 and 210 a) were weak before the Holocene, strongest in the early and middle Holocene, and gradually weakened during the late Holocene (Fig. 5b). This variation also shows the complexity of regional climate change over a long time-scale.

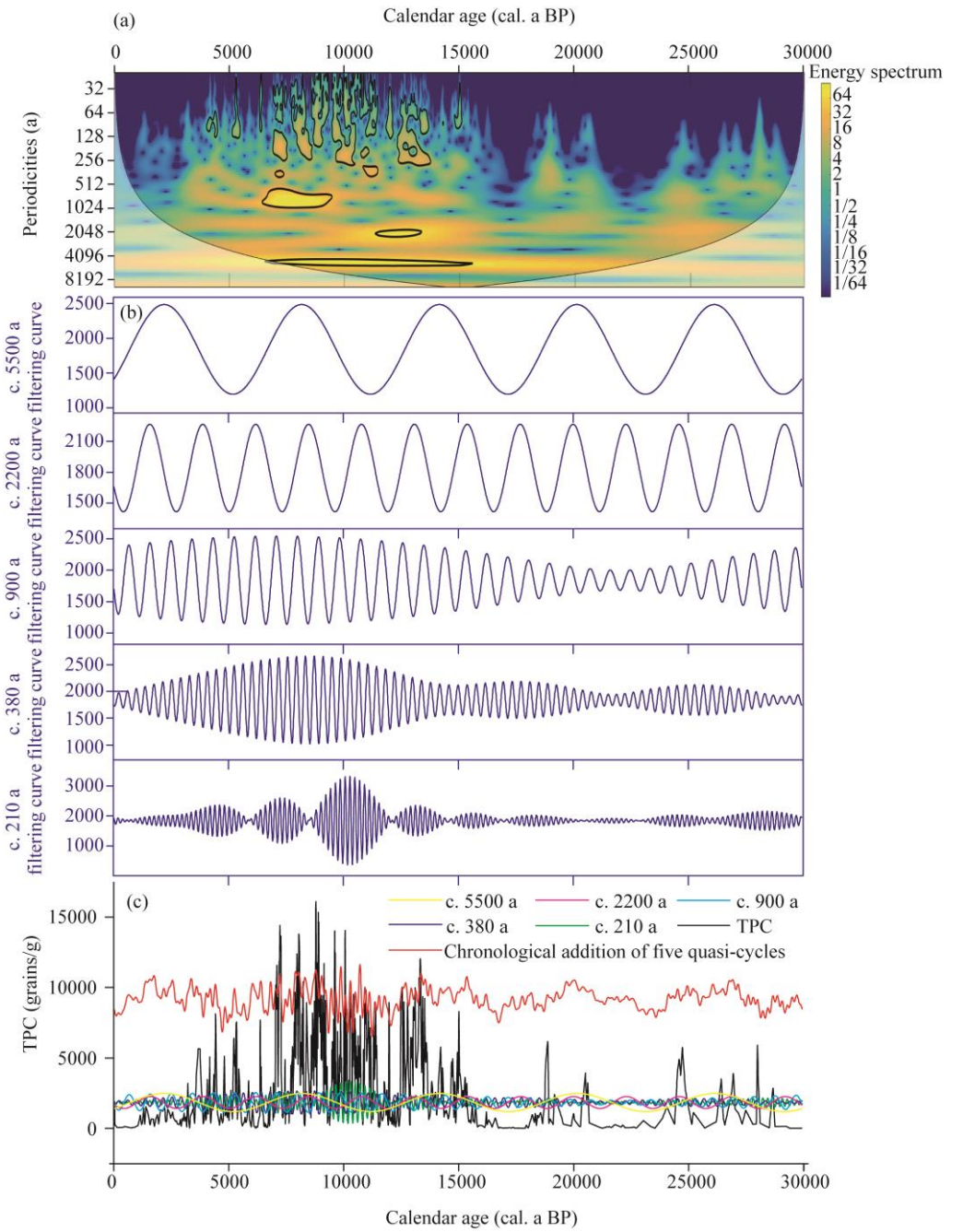

Fig. 5 Wavelet analysis results and filtering analysis curve of the total pollen concentration (TPC) series for the past 30 ka in the XG (Xiaogou) section. (a), wavelet analysis results (yellow, high energy spectrum; blue, low energy spectrum; black line, more than 95% confidence); (b), filtering curve of the principal periodic components; (c), TPC curve.

In summary, the cold-dry climate events (H3, H2, H1, the Younger Dryas, and the Holocene cold-dry events, etc.) revealed by the high-resolution multi-proxy (Md, TOC, and TPC, etc.) from the XG section, are comparable to those noted in other records, such as the deep-sea sediments in the North Atlantic, Greenland ice cores, and stalagmites from the Hulu Cave and Dongge Cave, indicating the teleconnection of climate change between mid-latitudes, and high and low latitudes. TPC curve from the XG section is parallel to the summer solar radiation curve in the mid-latitudes of the Northern Hemisphere, and the millennial- and centennial-scale quasi-cycles

(i.e., c. 2200, 900, 380, and 210 a) from wavelet analysis on TPC also align with the millennial- to centennial-scale quasi-cycles in solar activity, indicating that the source driving force of climate change may be solar radiation activity.

5 Conclusions

We analyzed high-resolution multi-proxy records (particle size, TOC, and pollen record) from an alluvial-lacustrine-aeolian sequence (i.e., XG section) based on the improved age-depth model in the western Chinese Loess Plateau, situated in the north-western margin of the East Asian monsoon region. Our study revealed that the late stage of the last glacial from 30.1 to 18.1 cal. ka BP was generally a rather dry and cold period. Three Heinrich or Heinrich-like events (even drier and probably colder) occurred at 29.5, 23.8, and 19.7 cal. ka BP. The deglacial (from 18.1 to 11.5 cal. ka BP) was apparently a wetting (probably also warming) period. And, superimposed on the wetting trend were three cold and dry excursions, i.e., the Oldest Dryas (or Heinrich Event 1), the Older Dryas, and the Younger Dryas. The intervening intervals were two warm periods, i.e., the Bølling and the Allerød warm period. The Holocene can be divided into three portions: the warmest and wettest early portion from 11.5 to 6.7 cal. ka BP, the dramatically dried and cooled middle portion from 6.7 to 3.0 cal. ka BP, and the driest and coldest late portion since 3.0 cal. ka BP. Eleven dry and cold episodes were superimposed on these general patterns. Wavelet analysis results on TPC revealed five significant or high-confidence periodicities. Except for c. 5500 a quasi-cycle that is similar to the Heinrich events, the other four quasi-cycles (i.e., c. 2200, 900, 380, and 210 a) are most likely indirectly associated with solar activities. This study provides an important scientific reference for further in-depth discussion of the mechanisms of regional climate change and prediction of future trends in climate and environmental change.

Acknowledgements

This work was funded by the National Natural Science Foundation of China (41662013, 40025105, 41972020). The authors thank Prof. FENG Zhaodong from Henan University, China for constructive comments on the manuscript. We are grateful to Prof. MA Yuzhen, Dr. WU Jing, Mr. GAO Weidong, and Mr. ZHENG Peng for participating the field sampling work. We are also indebted to Dr. SUN Aizhi and Mr. LI Fei for completing a part of pollen analysis, and Ms. KUANG Juan for the particle-size and TOC analysis. Especially, Dr. WANG Jianglin gives us good help and guidance in data processing of wavelet analysis.

References

An Z S, Colman S M, Zhou W J, et al. 2012. Interplay between the westerlies and Asian monsoon recorded in lake Qinghai sediments since 32 ka. Scientific Reports, 2(8): 619, doi: 10.1038/srep00619.

Arbic B K, MacAyeal D R, Mitrovica J X, et al. 2004. Palaeoclimate: Ocean tides and Heinrich events. Nature, 7016: 432460, doi: 10.1038/432460a.

Berger A L. 1978. Long-term variations of caloric insolation resulting from the Earth's orbital elements. Quaternary Research, 9(2): 139–167.

Bezrukova E V, Tarasov P E, Kulagina N V, et al. 2011. Palynological study of Lake Kotokel' bottom sediments (Lake Baikal region). Russian Geology and Geophysics, 52(4): 458–465.

Bond G, Showers W, Cheseby M, et al. 1997. A pervasive millennial-scale cycle in north Atlantic Holocene and glacial climates. Science, 278(5341): 1257–1266.

Bond G, Showers W, Elliot M, et al. 1999. The North Atlantic's 1-2 kyr climate rhythm: Relation to Heinrich Event, Dansgaard-Oeschger cycles and the Little Ice Age. Geophysical Monograph, 112: 35–58.

Chen F H, Bloemendal J, Feng Z D, et al. 1999. East Asian monsoon variations during oxygen isotope stage 5: Evidence from the northwestern margin of the Chinese Loess Plateau. Quaternary Science Reviews, 18(8–9): 1127–1135.

Chen F H, Zhu Y, Li J J, et al. 2001. Abrupt Holocene changes of the Asian Monsoon at millennial and centennial-scales: Evidence from lake sediment document in Minqin Basin, NW China. Chinese Science Bulletin, 46: 1942–1947.

Chen F H, Cheng B, Zhao Y, et al. 2006. Holocene environmental change inferred from a high-resolution pollen record, Lake Zhuyeze, arid China. The Holocene, 16(5): 675–684.

Chen J A, Wan G J, David D Z, et al. 2004. Environmental records of lacustrine sediments in different time scales: Sediment grain size as an example. Science in China Series D-Earth Sciences, 47(10): 954–960.

Chen Y P, Lin S C, Xu Y R. 2000. The natural appearance and origin of agriculture and animal husbandry in mid-Gansu during the pre-Qin period. Journal of Tianshui Normal University, 20(4): 70–74. (in Chinese)

Clemens S C. 2005. Millennial-band climate spectrum resolved and linked to centennial-scale solar cycles. Quaternary Science Reviews, 24(5–6): 521–531.

Debret M, Sebag D, Crosta X, et al. 2009. Evidence from wavelet analysis for a mid-Holocene transition in global climate forcing. Quaternary Science Reviews, 28(25–26): 2675–2688.

Ding Z L, Ren J Z, Liu D S, et al. 1996. The mechanisms of the millennium-scale irregular change of the late Pleistocene monsoon-desert system. Science of China (Series D), 26(5): 385–391. (in Chinese)

Dykoski C A, Edwards R L, Cai C, et al. 2005. A high-resolution, absolute-dated Holocene and deglacial Asian monsoon record from Dongge Cave, China. Earth & Planetary Science Letters, 233(1–2): 71–86.

Grimm E C, Jacobson Jr G L, Watts W A, et al. 1993. A 50,000-year record of climate oscillations from Florida and its temporal correlation with the Heinrich Events. Science, 261(5118): 198–200.

Grootes P M, Stuiver M, White J W C, et al. 1993. Comparison of oxygen isotope records from the GISP2 and GRIP Greenland ice cores. Nature, 366: 552–554.

Guo X L, Wang Q, Shi J A, et al. 2002. Characters of the total organic carbon and organic carbon isotope and grain size and paleoclimate significance in Qinghai lake sediments. Marine Geology & Quaternary Geology, 22(3): 99–103. (in Chinese)

Huang C J, Tian X L. 2018. Discussion on the driving mechanism of solar activity to interannual-suborbital-scale climate change. Quaternary Sciences, 38(5): 1255–1267. (in Chinese)

Kravchinsky V A, Langereis C G, Walker S D, et al. 2013. Discovery of Holocene millennial climate cycles in the Asian continental interior: has the sun been governing the continental climate? Global and Planet Change, 110: 386–396.

Kravchinsky V A, Zhang R, Borowiecki R, et al. 2021. Centennial scale climate oscillations from southern Siberia in the Last Glacial Maximum. Quaternary Science Reviews, 270: 107–171.

Li S, Qiang M R, Li B S, et al. 2004. Rapid climate changes at northwestern margin of East Asian monsoon region during the last deglaciation. Geological Review, 50(1): 106–112. (in Chinese)

Li X Q, Zhou W J, An Z S, et al. 2000. Palaeovegetation record of monsoon evolution in desert-loess transition zone since 13 ka BP. Acta Botanica Sinica, 42(8): 868–872. (in Chinese)

Li X Q, Zhou W J, An Z S, et al. 2003. The vegetation and monsoon variations at the desert-loess transition belt at Midiwan in northern China for the last 13 ka. The Holocene, 13(5): 779–784.

Liu J Q, Ni Y Y, Chu G Q. 2001. Main palaeoclimatic events in the Quaternary. Quaternary Sciences, 21(3): 239–248. (in Chinese)

Luo C X, Pan A D, Zheng Z. 2006. Progresses about the studies on the relationship between topsoil spore-pollen and vegetation in arid areas of Northwest China. Arid Zone Research, 23(2): 314–319. (in Chinese)

Ojala A E K, Launonen I, Holmstrom L, et al. 2015. Effects of solar forcing and North Atlantic oscillation on the climate of continental Scandinavia during the Holocene. Quaternary Science Reviews, 112: 153–171.

Reimer P J. 2020. Composition and consequences of the IntCal20 radiocarbon calibration curve. Quaternary Research, 96: 22–27.

Ren G Y, Jiang D B, Yan Q. 2021. Characteristics, drivers and feed backs of paleo-climatic variations and the implications for modern climate change research. Quaternary Sciences, 41(3): 824–841. (in Chinese)

Shen J, Liu X Q, Wang S M, et al. 2005. Palaeoclimatic changes in the Qinghai Lake area during the last 18,000 years. Quaternary International, 136: 131–140.

Shen J, Xue B, Wu J L, et al. 2010. Lake Sediments and Environmental Evolution. Beijing: Science Press, 143–242. (in Chinese)

Soon W, Herrera V M V, Selvaraj K, et al. 2014. A review of Holocene solar linked climatic variation on centennial to millennial timescales: Physical processes, interpretative frameworks and a new multiple cross-wavelet transform algorithm. Earth-Science Reviews, 134: 1–15.

Stuiver M, Grootes P M, Braziunas T F. 1995. The GISP2 $\delta^{18}O$ climate record of the past 16,500 years and the role of the sun, ocean, and volcanoes. Quaternary Research, 44(3): 341–354.

Sun A Z, Feng Z D. 2015. Climatic changes in the western part of the Chinese loess plateau during the last deglacial and the Holocene: A synthesis of pollen records. Quaternary International, 372: 130–141.

Tang L Y, Li C H, An C B, et al. 2007. Vegetation history of the western Loess Plateau of China during the last 40 ka based on pollen record. Acta Palaeontologica Sinica, 46(1): 45–61. (in Chinese)

Tarasov P E, Bezrukova E V, Krivonogov S K. 2009. Late Glacial and Holocene changes in vegetation cover and climate in southern Siberia derived from a 15 kyr long pollen record from Lake Kotokel. Climate of the Past, 5(3): 285–295.

Torrence C, Compo G P. 1998. A practical guide to wavelet analysis. Bulletin of the American Meteorological Society, 79(1): 61–78.

Wang P X. 2009. Global monsoon in a geological perspective. Chinese Science Bulletin, 54(7): 1113–1136.

Wang Y J, Cheng H, Edwards R L, et al. 2001. A high-resolution absolute-dated late Pleistocene monsoon record from Hulu Cave, China. Science, 294(5550): 2345–2348.

Wu H N, Ma Y Z, Feng Z D, et al. 2009. A high resolution record of vegetation and environmental variation through the last 25,000 years in the western part of the Chinese Loess Plateau. Palaeogeography, Palaeoclimatology, Palaeoecology, 273(1–2): 191–199.

Wu H N, Zhang C X, Zhao H K, et al. 2020. Vegetation succession and its response to climate changes since the Last Glacial Maximum on the Loess Plateau of central Gansu, Northwest China. Chinese Journal of Ecology, 39(8): 2488–2500. (in Chinese)

Wu Z Y, Hou X Y, Zhu Y C, et al. 1980. Vegetation of China. Beijing: Science Press, 731–745. (in Chinese)

Xia Z K. 1992. Underwater loess and paleoclimate. Acta Geographica Sinica, 47(1): 58–65. (in Chinese)

Yang S L, Dong X X, Xiao J L. 2019. The East Asian monsoon since the Last Glacial Maximum: Evidence from geological records in Northern China. Science China Earth Sciences, 62: 1181–1192.

Zeng Y L, Chen S T, Yang S H, et al. 2019. Multiscale analysis of Asian Monsoon over the past 640 ka. Science China Earth Sciences, 62: 843–852.

Zhang Z P, Huang W, Chen J H, et al. 2017. Multi-time scale analysis of East Asian summer monsoon and its possible mechanism during Holocene. Quaternary Sciences, 37(3): 498–509. (in Chinese)

Zhao X H, Feng X S. 2014. Periodicities of solar activity and the surface temperature variation of the Earth and their correlations. Chinese Science Bulletin, 59(14): 1284–1292. (in Chinese)

Zhou W J, Donahue D J, Porter S C, et al. 1996. Variability of monsoon climate in East Asia at the end of the last glaciation. Quaternary Research, 46(3): 219–229.

Zhou W J, Head M L, Lu X F, et al. 1999. Teleconnection of climatic events between East Asia and polar, high latitude areas during the last deglaciation. Palaeogeography, Palaeoclimatology, Palaeoecology, 152(1–2): 163–172.

Zhu Y. 2002. Study on Holocene lake pollen records and environmental changes in Shiyang River basin. PhD Dissertation. Lanzhou: Lanzhou University. (in Chinese)